JES Focus Issue of Selected Papers from IMLB 2018

Improvement of Li-Sulfur Cell Cycling Performance by Use of $Fe_{1-x}S$@NC as a Functional Additive for Chemical Confinement of Lithium Polysulfides

Jun Hwan Ahn, Ganesh Kumar Veerasubramani,* Sang-Min Lee, Tae-Sun You, and Dong-Won Kim **,z

Department of Chemical Engineering, Hanyang University, Seongdong-Gu, Seoul 04763, Korea

Lithium-sulfur cells using sulfur as an active cathode material offer high energy density and low-cost. However, dissolution and migration of lithium polysulfides (the 'shuttle effect') remain key obstacles for the practical development of lithium-sulfur cells. Here, we demonstrate that $Fe_{1-x}S$ (pyrrhotite) coated by N-doped carbon ($Fe_{1-x}S$@NC) with high affinity for polysulfides and high electronic conductivity can be used as a functional additive to trap lithium polysulfides and reutilize reaction intermediates in the sulfur cathode during cycling. The addition of $Fe_{1-x}S$@NC into the sulfur cathode results in the enhancement of cycling performance of the lithium-sulfur cell in terms of initial discharge capacity, capacity retention and rate capability. This superior cycling performance can be attributed to strong chemical interactions between electrically conductive $Fe_{1-x}S$@NC particles and lithium polysulfides, which suppress the dissolution of lithium polysulfides and enhance the utilization of active sulfur during repeated cycling.
 [DOI: 10.1149/2.0311903jes]

Manuscript submitted October 24, 2018; revised manuscript received December 4, 2018. Published December 20, 2018. *This paper is part of the JES Focus Issue of Selected Papers from IMLB 2018.*

After more than two decades of dedicated research and development, lithium-ion batteries have attained huge commercial successes and are used in various applications from portable electronic devices to electric vehicles. However, the growing demand for large-scale energy storage systems requires significant improvements in energy density and further reduction in battery cost.[1–4] Among the various types of next generation lithium batteries, lithium-sulfur batteries have attracted considerable attention owing to their high theoretical energy density, low price and environmentally friendliness. However, their practical application is inhibited by several problems, including large volume change, low electronic conductivity of active sulfur and dissolution of lithium polysulfide intermediates (Li_2S_x, $4 \leq x \leq 8$) into electrolytes.[5–7] Large volumetric changes can be mitigated by designing cathodes with a porous structure, and the electronic conductivity of sulfur and reaction intermediates can be enhanced by addition of large amount of conducting carbon, although this also results in a decrease in the energy density. The use of a physical barrier and anchor for polysulfide intermediates has suppressed the dissolution and migration of lithium polysulfides. One of the successfully implemented approaches is to suppress polysulfide migration by infiltrating molten sulfur into a mesoporous carbon structure.[8] Since this was first reported, other attempts to physically block the migration of lithium polysulfides from the sulfur cathode to the lithium anode through electrolyte solution have been reported.[9–21] The physically blocking concept was effective to some extent, but could not achieve good long-term cycling stability, which rendered chemical adsorption more attractive. Various materials utilizing chemical interactions between polysulfides and doped carbon,[22–25] carbon with polar functional groups[26–28] and graphitic nitrides[29] have been actively investigated. These conductive carbonaceous materials can offer many reaction sites for lithium polysulfides to be reutilized during subsequent cycles, but their interaction with polysulfides is significantly weaker than that with metal oxides. On the other hand, metal oxides have a high affinity with polysulfides owing to strong metal-sulfur interaction derived from the Lewis acid-base interaction.[30–32] However, their electronic conductivity is significantly low, compelling polysulfides to move toward electronically conductive sites before they participate in electrochemical reactions, making it difficult for adsorbed polysulfides to be reutilized during charge and discharge cycles.[33] Accordingly, additives with high electronic conductivity and strong affinity to polysulfides are essential to further improve the cycling performance of lithium-sulfur cells. In this respect, metal sulfides can be good candidate materials.[34–39] Not only do they exhibit higher electronic conductivity than metal oxides, but they also have a strong affinity with polysulfides owing to Lewis acid-base interactions between metal cations and polysulfide anions.

In this work, we synthesized an $Fe_{1-x}S$ particle coated by N-doped carbon ($Fe_{1-x}S$@NC) and proposed it as a functional additive for chemical confinement of polysulfides in the sulfur cathode. These $Fe_{1-x}S$@NC particles exhibited higher electronic conductivity compared with their precursor metal oxide (Fe_2O_3) and higher adsorption ability toward lithium polysulfides than do Fe_2O_3 and other carbonaceous materials such as Super-P and multi-wall carbon nanotube (MWCNT). As a result, the lithium-sulfur cell with $Fe_{1-x}S$@NC as an additive in the sulfur cathode exhibited better cycling performance than did cells with pristine sulfur and Fe_2O_3-added sulfur cathodes.

Experimental

Preparation of Fe_2O_3 particles.—The facile precipitation method was used to prepare Fe_2O_3 particles.[40] Firstly, 1.0 M of ferric chloride ($FeCl_3$, Sigma Aldrich) was dissolved in 50 ml ethanol and kept at 70°C with constant stirring. Subsequently, 50 ml of 2.5 M sodium hydroxide (NaOH, Sigma Aldrich) aqueous solution was added to the above solution and stirred for 1 h. Then, the mixture was transferred to an electric oven and heated to 100°C for 4 days. After that, the dark orange-colored precipitate was collected by centrifugation and washed with deionized water and ethanol several times to remove impurities. Finally, Fe_2O_3 particles could be obtained by drying at 80°C for 12 h in a vacuum oven.

Synthesis of $Fe_{1-x}S$@NC particles.—A mixture of prepared Fe_2O_3 particles (0.5 g) and dopamine hydrochloride (0.2 g, $C_8H_{11}NO_2 \cdot HCl$, Sigma Aldrich) was dispersed in 250 mL of Tris-buffer solution (Sigma Aldrich) with continuous stirring for 5 h. Then, the resulting product was collected via centrifugation and washed with deionized water and ethanol three times. It was then dried at 70°C for 12 h in the oven. The obtained Fe_2O_3@polydopamine (PDA) particles were mixed with thioacetamide (C_2H_5NS, Sigma Aldrich) in a weight ratio of 1:3 and the mixture was transferred to an alumina boat. The sample loaded in the alumina boat was moved to a tube furnace and

*Electrochemical Society Student Member.
**Electrochemical Society Member.
zE-mail: dongwonkim@hanyang.ac.kr

Table I. Composition of electrode components in different types of cathodes.

Electrode	Sulfur (wt%)	Fe_2O_3 (wt%)	$Fe_{1-x}S$@NC (wt%)	Super-P (wt%)	PVdF (wt%)
Sulfur	60	-	-	30	10
Sulfur + Fe_2O_3	60	15	-	15	10
Sulfur + $Fe_{1-x}S$@NC	60	-	15	15	10

kept at 500°C for 5 h under an argon atmosphere to induce both sulfurization of Fe_2O_3 and carbonization of PDA. The same procedure was followed to prepare $Fe_{1-x}S$ by direct sulfurization of Fe_2O_3 with thioacetamide.

Electrode preparation and cell assembly.—Sulfur powder (Sigma-Aldrich), $Fe_{1-x}S$@NC, Super-P carbon (MMM co.) and poly(vinylidene fluoride) (PVdF, Solef 5130, Solvay) binder were dispersed in *N*-methyl pyrrolidinone (NMP, Sigma-Aldrich) at a mass ratio of 60/15/15/10 to prepare the viscous slurry for sulfur cathode. For comparison, the same amount of $Fe_{1-x}S$@NC was substituted with Fe_2O_3 and Super-P for making sulfur+Fe_2O_3 and sulfur only electrode, respectively. The content of electrode components in different types of cathodes is given in Table I. The obtained slurry was coated onto carbon-coated aluminum foil using a doctor blade and dried at 60°C for 15 h in a vacuum oven. The mass loading of active sulfur in the sulfur cathode was about 2.0 mg cm^{-2}. The lithium anode was prepared by pressing 200 μm-thick lithium foil (Honjo Metal Co. Ltd.) onto a copper current collector. The Li-sulfur cell was assembled by sandwiching a polyethylene separator (Asahi ND420, thickness: 20 μm) between the lithium anode and the sulfur cathode in a CR2032-type coin cell. The cell was then injected with a liquid electrolyte (80 μl) consisting of 1.0 M lithium bis(trifluoromethanesulfonyl)imide ($LiN(SO_2CF_3)_2$, LiTFSI) dissolved in a mixed solvent of 1,3-dioxolane (DOL) and 1,2-dimethoxyethane (DME) (50:50 by volume) containing 0.4 M $LiNO_3$ as an additive (battery grade, PANAX ETEC Co. Ltd.). All cells were assembled in a globe box filled with argon gas to avoid water and oxygen contamination.

Characterization and measurements.—Morphological analysis was performed using a scanning electron microscope (JEOL JSM 6701F). A high-resolution transmission electron microscope (HRTEM, JEOL, JEOL-2100F) was used to obtain morphologies, lattice fringe patterns and electron diffraction (SAED) patterns for selected areas of the $Fe_{1-x}S$@NC particles. Surface elemental mapping of $Fe_{1-x}S$@NC particle was conducted using an energy dispersive X-ray spectrometer (EDS) attached to a TEM. X-ray diffraction (XRD) patterns were recorded using a Rigaku miniFlex600 using Cu (λ = 0.15 nm) radiation. To compare the polysulfide adsorption ability of $Fe_{1-x}S$@NC particles with multi-walled carbon nanotube (MWCNT, CM-150, Hanhwa Chemical), Super-P carbon and Fe_2O_3, Li_2S_4 was synthesized according to the procedure previously reported.[31] For the polysulfide adsorption test, 5 mg of Li_2S_4 powder was dissolved in 5 ml of tetrahydrofuran (THF) and 20 mg of test material (MWCNT, Super-P, Fe_2O_3, $Fe_{1-x}S$@NC) was added into the solution and stirred for 10 min. A digital photograph of the solution was taken after 6 min, 1 h and 6 h to monitor the color change of the solution. The electronic conductivities of Fe_2O_3 and $Fe_{1-x}S$@NC were measured using the 4-point probe method. Each powder was ground together with KBr in a weight ratio of 1:3 and the mixture was placed into the IR pelletizer. We applied 3000 MPa to the IR pelletizer using an oil-hydraulic press for 3 min. Charge and discharge cycling tests of the Li-sulfur cells were carried out in the voltage rage of 1.8 to 2.6 V at a constant current rate of 0.2 C (335 mA g^{-1}_{sulfur}) and at 25°C using battery testing equipment (WBCS 3000, WonATech Co., Ltd.). Electrochemical impedance spectroscopy was performed using a Zahner Electrik IM6 impedance analyzer. The frequency range was from 100 kHz to 100 mHz with an AC voltage amplitude of 10 mV.

Results and Discussion

Figure 1a presents the TEM image of synthesized $Fe_{1-x}S$@NC particles, showing an irregular spherical shape with an average particle size less than 1 μm. A magnified image of a single $Fe_{1-x}S$@NC particle is given in Figure 1b, illustrating a core-shell structure with N-doped carbon coated on the surface of the $Fe_{1-x}S$ core particle. Here, the N-doped carbon coating layer on $Fe_{1-x}S$ was formed by the polymerization of dopamine, followed by carbonization under an inert atmosphere. The thickness of the coating layer was measured to be about 27 nm. No distinct lattice fringe patterns could be observed in the coating layer on the $Fe_{1-x}S$@NC particle (Figure 1c), indicating an amorphous nature of the N-doped carbon.[41] Lattice fringe patterns of $Fe_{1-x}S$ core particles could be identified and the corresponding lattice spacing was about 0.45 nm. The SAED pattern in Figure 1d shows the N-doped carbon layer with diminished bright $Fe_{1-x}S$ rings. This confirms that $Fe_{1-x}S$@NC has a polycrystalline nature with imperceptible rings. Figures 2b–2f show element mappings of an $Fe_{1-x}S$@NC particle with its TEM image (Figure 2a); these confirm that all elements (i.e., Fe, S, C, and N) are uniformly distributed in the $Fe_{1-x}S$@NC particle. These results indicate the successful synthesis of core-shell structured $Fe_{1-x}S$@NC particles consisting of a polycrystalline $Fe_{1-x}S$ core and amorphous N-doped carbon-coating layer.

The crystalline structures of the prepared materials were characterized by X-ray diffraction (XRD) analysis. Figure 3a shows the XRD patterns of the Fe_2O_3, $Fe_{1-x}S$ and $Fe_{1-x}S$@NC particles. The XRD pattern of the Fe_2O_3 particles presents well-defined crystalline peaks at 24.1°, 33.1°, 35.6°, 40.8°, 49.4°, 54.0°, 62.4° and 64.0°, corresponding to the orthorhombic crystal structure; all the diffraction peaks were well matched with JCPDS card no: 89-2810. The diffraction peaks observed in the $Fe_{1-x}S$ and $Fe_{1-x}S$@NC particles could be unambiguously assigned to the hexagonal phase of $Fe_{1-x}S$ without any impurity peaks or other phases, indicating that Fe_2O_3 particles were converted to $Fe_{1-x}S$ phase during sulfurization. The crystalline peaks observed at 29.9°, 33.8°, 43.8°, 53.1°, 57.4°, 65.2°, 71.2° and 74.2° can be assigned to the (100), (101), (102), (110), (103), (201), (202), and (104) planes, respectively.[42] As shown in figure, the hexagonal phase of the $Fe_{1-x}S$ core in the $Fe_{1-x}S$@NC was well maintained even after carbonization at high temperature. No crystalline peaks for N-doped carbon could be observed in the XRD pattern of $Fe_{1-x}S$@NC, which reveals that the amorphous N-doped carbon was coated on the surface of the pyrrhotite $Fe_{1-x}S$ core particle. To further examine the chemical nature of the $Fe_{1-x}S$@NC particle, XPS analysis was performed. In Fe2p core-level spectrum (Figure 3b), two major peaks were observed at 710.8 and 724.5 eV, which are attributed to the $Fe2p_{3/2}$ and $Fe2p_{1/2}$, respectively.[43] The broad peaks at 163.6 and 164.8 eV in Figure 3c can be attributed to $S2p_{1/2}$ and $S2p_{3/2}$, respectively.[44] The presence of oxidized groups (SO_x) was identified at the high binding energy. C1s core-level spectrum in Figure 3d can be resolved into 284.7, 285.8 and 288.5 eV, which correspond to the C–C, C–N, C–O bonds, respectively. The N1s core-level spectrum shown in Figure 3e can be deconvoluted into three major peaks at the binding energies of 397.5, 399.5 and 400.5 eV, which are attributed to the pyridinic-N, pyrrolic-N and graphitic-N bonds, respectively.[45] To estimate the amount of carbon present in the $Fe_{1-x}S$@NC particle, TGA was performed and the result is presented in Figure 3f. The initial weight gain was caused by the partial conversion of $Fe_{1-x}S$ into $FeSO_4$, as previously reported.[46] The final weight loss can be ascribed to the decomposition of unreacted $Fe_{1-x}S$ and $FeSO_4$ into Fe_2O_3 and the decomposition of carbon into CO_2. From the TGA analysis, the amount of carbon present in the $Fe_{1-x}S$@NC particle was calculated to be 15.2%.

Polysulfide adsorption ability is one of the most important factors when choosing an appropriate material for chemical confinement of soluble lithium polysulfides formed in the sulfur cathode. To investigate the polysulfide adsorption ability of various materials, Li_2S_4 was chosen as a model polysulfide because it is the most commonly

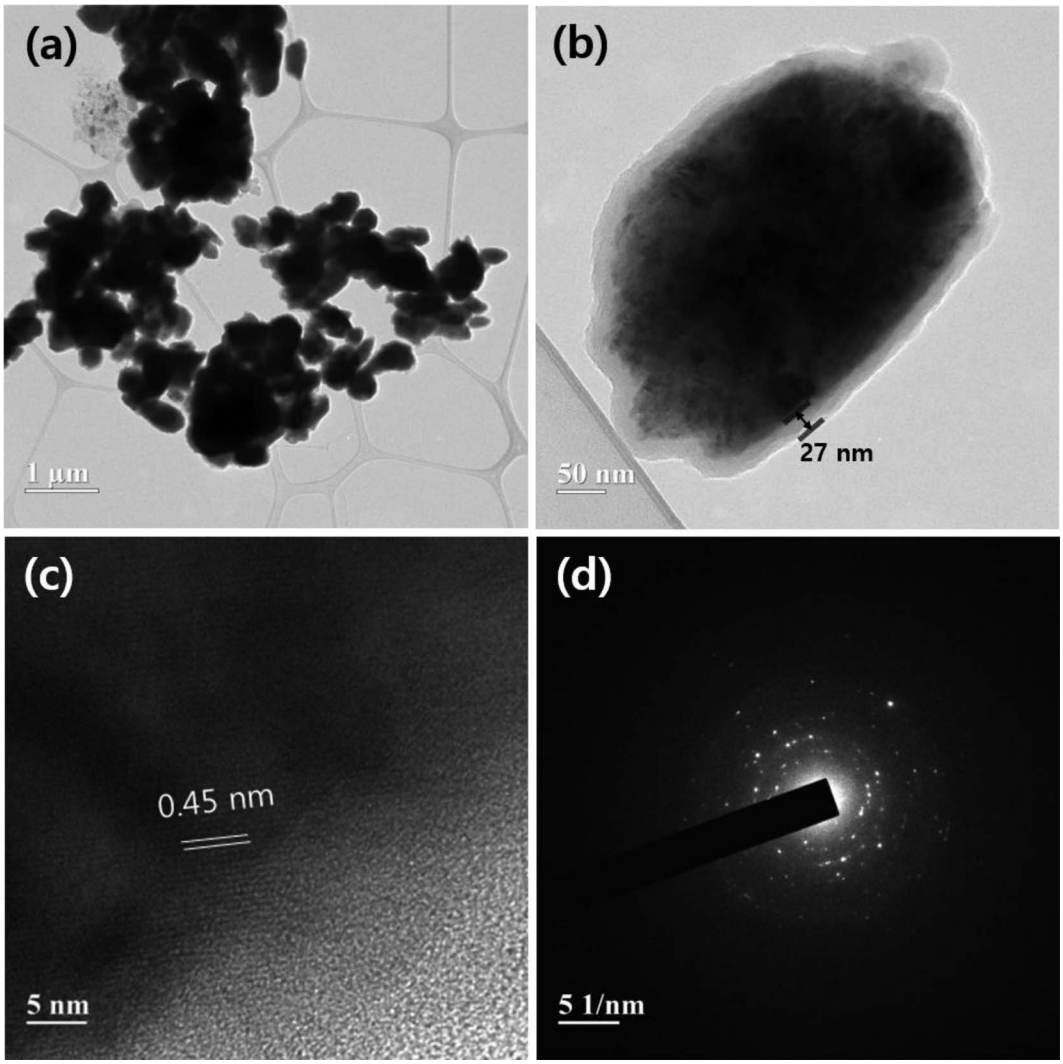

Figure 1. TEM images of synthesized $Fe_{1-x}S$@NC particles with (a) lower and (b) higher magnification. (c) High-resolution TEM image of $Fe_{1-x}S$@NC particle showing lattice fringe pattern and its line spacing, and (d) SAED pattern of $Fe_{1-x}S$ core particle showing its polycrystalline nature.

produced among the soluble lithium polysulfides (Li_2S_x, $4 \leq x \leq 8$) when sulfur is fully reduced to Li_2S during the discharge process. Another reason for choosing Li_2S_4 as a model polysulfide was that Li_2S_4 remains the longest in the electrolyte solution and its migration to the anode side would be the most probable among the soluble lithium polysulfides, since the reduction of Li_2S_4 into Li_2S is obviously the most sluggish step except for the solid-solid reaction of Li_2S_2 to Li_2S during the discharge process. To compare the polysulfide adsorption abilities of various materials, the color changes of Li_2S_4 solutions containing MWCNT, Super-P, Fe_2O_3 and $Fe_{1-x}S$@NC were monitored using a digital camera as a function of time. It should be noted that the amount of materials added into the vials of polysulfide solution are same (60 mg each). As shown in Figure 4, four types of test materials were floating in the Li_2S_4 solution and there was little color change in the solution after 0.1 h. However, we could clearly observe the difference in the color of the Li_2S_4 solutions after 6.0 h. When adding $Fe_{1-x}S$@NC into the Li_2S_4 solution, the color of the solution turned from yellow to colorless, indicating that most of Li_2S_4 in the solution was trapped by the $Fe_{1-x}S$@NC owing to strong interaction between $Fe_{1-x}S$@NC particles and Li_2S_4. On the other hand, the Li_2S_4 solution containing Fe_2O_3 remained light yellowish in color, implying a deficient ability of Fe_2O_3 to trap lithium polysulfides as compared with $Fe_{1-x}S$@NC. In contrast, the color of the Li_2S_4 solutions containing MWCNT and Super-P remained intact (yellow) after 6.0 h, which suggests that these carbonaceous materials could not adsorb the Li_2S_4 in the solution. BET surface area of $Fe_{1-x}S$@NC was measured to be 4.8 $m^2\ g^{-1}$, which is much lower than those of MWCNT and Super-P carbon. These results demonstrate that the adsorption ability of $Fe_{1-x}S$@NC is much higher than that of carbonaceous materials, even though it has a smaller surface area than MWCNT and Super-P carbon. The superior adsorption ability of $Fe_{1-x}S$@NC for lithium polysulfides arises from the Lewis acid-base interactions between $Fe_{1-x}S$@NC particles and polysulfides.

Electronic conductivity of an additive material for trapping lithium polysulfides is another crucial property in additives for chemical confinement, since the lithium polysulfides trapped by the additive must be reutilized during subsequent cycles. In this regard, the electronic conductivity of $Fe_{1-x}S$@NC and Fe_2O_3 should be measured and compared. However, their intrinsic electronic conductivity could not be measured directly, because pelletizing using these particles was not possible owing to their brittle nature. Instead, $Fe_{1-x}S$@NC or Fe_2O_3 was mixed with KBr in same weight ratio (1:3) to prepare the solid-state pellet for conductivity measurements. As a result, the pellet prepared with $Fe_{1-x}S$@NC particles showed considerably higher electronic conductivity (0.30 S cm^{-1}) than the Fe_2O_3-based pellet (0.01 S cm^{-1}), indicating the higher electronic conductivity of $Fe_{1-x}S$@NC as compared with Fe_2O_3 particles. It should be noted that the electronic conductivity of $Fe_{1-x}S$@NC must be significantly

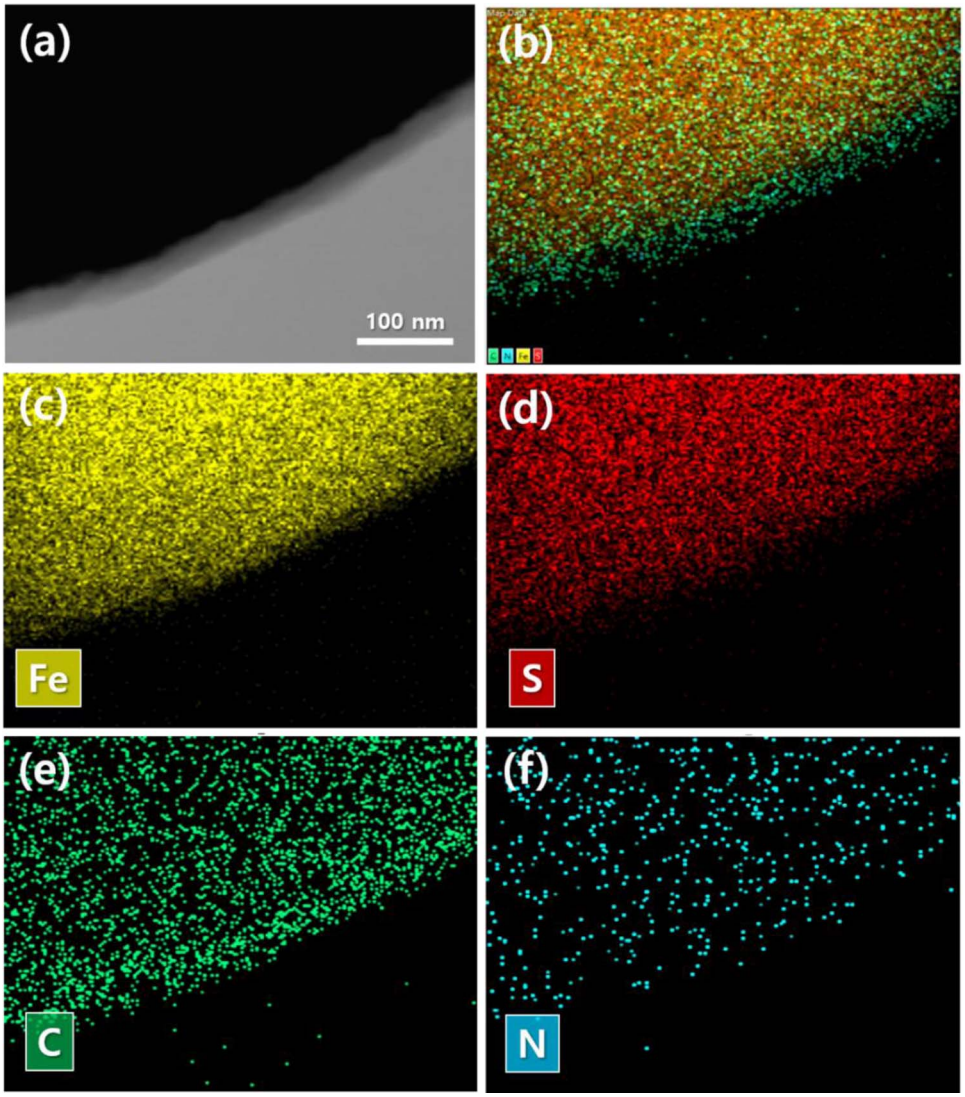

Figure 2. (a) TEM image of $Fe_{1-x}S$@NC particle showing existence of N-doped carbon coating layer surrounding $Fe_{1-x}S$ core particle. (b) Overall EDS mapping of $Fe_{1-x}S$@NC particle and individual EDS mapping images of (C) Fe, (d) S, (e) C and (f) N.

higher than the measured value (0.30 S cm^{-1}), since the pellet for the conductivity measurement contained high amounts (75 wt%) of KBr, which is electronically non-conductive. According to a previous study,[47] the electronic conductivity of $Fe_{1-x}S$ is in the range of 200 to 1,000 S cm^{-1}. It has been reported that the electronic conductivity of 10^{-1} S cm^{-1} is enough for materials to be used as cathode active materials.[48] Figure 5 shows the SEM image of the sulfur cathode containing $Fe_{1-x}S$@NC particles and corresponding EDS elemental mapping images. The sulfur electrode is uniform and highly porous, both of which are necessary for good accessibility of liquid electrolyte into the electrode and good accommodation of large volume change during repeated cycles. Elemental mapping images of S, Fe and N in Figures 5b–5d demonstrate that $Fe_{1-x}S$@NC particles were mixed well with active sulfur material and were uniformly distributed throughout the sulfur cathode.

The cycling performance of the Li-sulfur cells assembled with different cathodes was evaluated in the voltage range of 1.8 to 2.6 V at a constant current rate of 0.2 C, and the resulting charge-discharge voltage profiles are given in Figures 6a–6c. The voltage profiles exhibit two discharge plateaus and a long charge plateau. The discharge plateaus at around 2.35 and 2.10 V correspond to the reduction of elemental sulfur to higher order lithium polysulfides (Li_2S_x, $4 \leq x \leq 8$) that are soluble in the electrolyte and the reduction of long-chain polysulfides to insoluble Li_2S, respectively. The long charge plateau arises from the oxidation of Li_2S to cyclic sulfur. It can be clearly seen that the capacity delivered during lower discharge plateau was the highest in the Li-sulfur cell with $Fe_{1-x}S$@NC. This result suggests that most of the soluble lithium polysulfides formed in the sulfur cathode are trapped by $Fe_{1-x}S$@NC particles and reutilized for the subsequent reaction to produce Li_2S from the trapped lithium polysulfides during the lower discharge plateau period. While the cells with Fe_2O_3 and $Fe_{1-x}S$@NC exhibited similar capacity during the higher discharge plateau, there was a large difference in discharge capacity during the lower discharge plateau. Moreover, the second discharge plateau observed in the cell with Fe_2O_3 was not flat, implying unstable formation of Li_2S from the lithium polysulfides due to the electronically insulating nature of Fe_2O_3. As a result, the Li-sulfur cell with $Fe_{1-x}S$@NC delivered the higher initial discharge capacity (999.0 mAh g^{-1}) based on the mass of only sulfur material in the cathode. It should be noted that the reversible capacity of $Fe_{1-x}S$@NC material is very low in the voltage range of 1.8 to 2.6 V, and thus the contribution of the $Fe_{1-x}S$@NC to the specific capacity of the sulfur electrode is negligible. As shown in figures, the initial discharge capacity of the cell without any additives was the lowest (694.8 mAh g^{-1}), indicating that large amount of lithium polysulfides were dissolved into the electrolyte solution and migrated to the anode side. Cycling

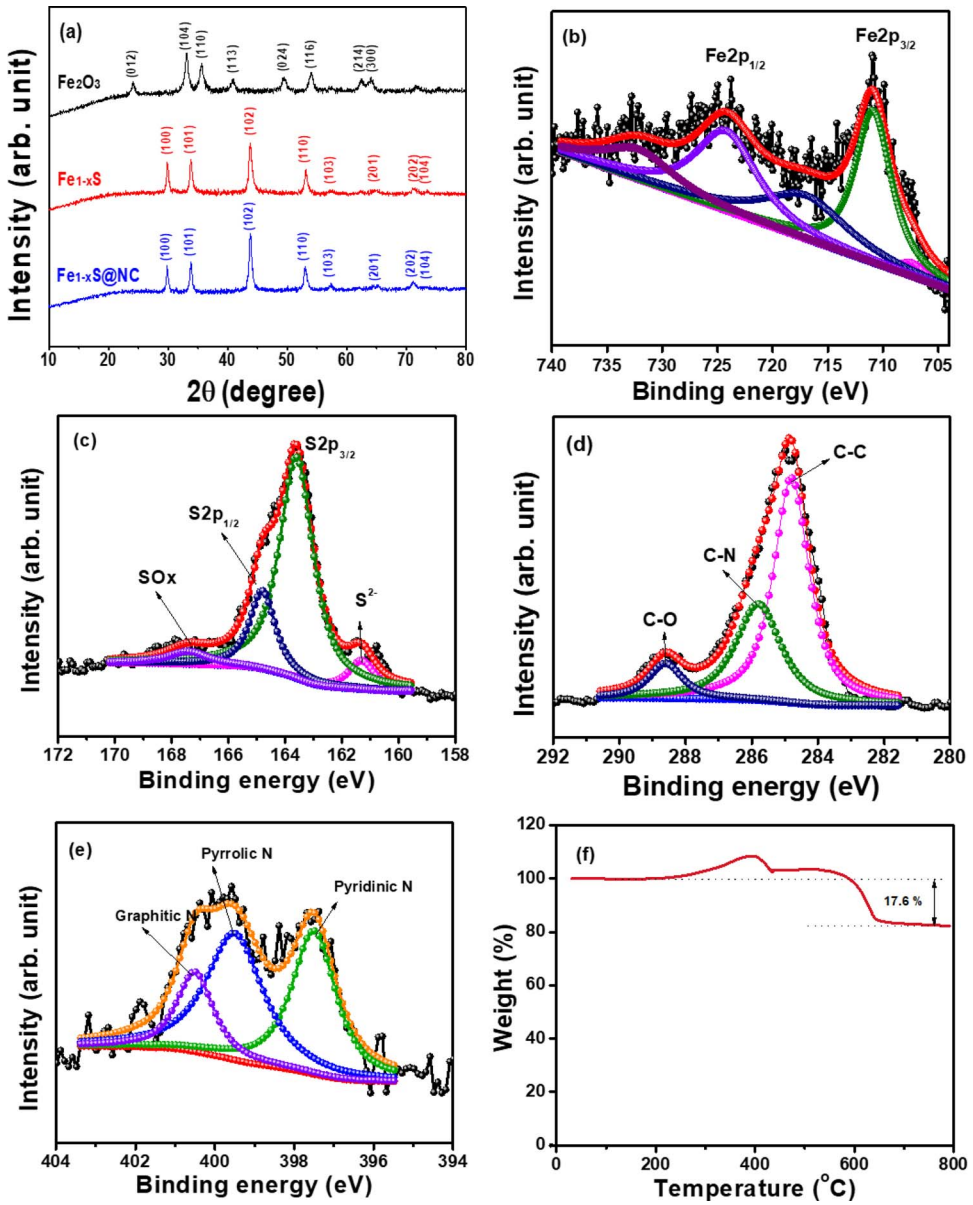

Figure 3. (a) XRD patterns of Fe_2O_3, $Fe_{1-x}S$ and $Fe_{1-x}S$@NC particles. XPS spectra of the (b) Fe2p core-level, (c) S2p core-level, (d) C1s core-level and (e) N1s core-level of $Fe_{1-x}S$@NC. (f) TGA curve of the $Fe_{1-x}S$@NC material.

performance of the Li-sulfur cells with different electrodes is compared in Figure 6d. The Li-sulfur cell without any additives showed a large capacity fading with cycling, which can be attributed to the gradual loss of active sulfur from the sulfur cathode. Although the Li-sulfur cell with Fe_2O_3 exhibited higher discharge capacity and better cycling stability as compared with the cell without additive, its capacity retention was inferior to the cell with $Fe_{1-x}S$@NC. The Li-sulfur cell with $Fe_{1-x}S$@NC delivered high discharge capacities throughout cycling and exhibited the best capacity retention (74.8% of its initial capacity) among the cells after 300 cycles. In addition, the cell with $Fe_{1-x}S$@NC showed the higher coulombic efficiency than any other cells during cycling. As discussed, most of the lithium polysulfides can be trapped in the sulfur cathode containing $Fe_{1-x}S$@NC; they can then be reutilized in subsequent cycles, which results in stable cycling and high coulombic efficiency.

To understand the cycling behavior of cells with different sulfur cathodes, AC impedance measurements of the cells were conducted after the 1st and 300th cycles. As shown in Figure 7, all cells showed two overlapping semicircles with a real axis intercept. The X-axis intercept observed at the highest frequency corresponds to the electrolyte resistance, the first semicircle in the high frequency range can be ascribed to Li^+ ion migration through the surface film on the electrode, and the second semicircle in the middle to low-frequency range is related with charge transfer reaction at the electrode-electrolyte interface. The three different resistances were designated as electrolyte resistance (R_e), film resistance (R_f) and charge transfer resistance (R_{ct}). When the first cycle was finished, all three cells exhibited similar resistances. However, the electrolyte resistances were found to increase after cycling. An increase in electrolyte resistance in the Li-sulfur cell can mainly be ascribed to the increase in viscosity of electrolyte solution due to gradual dissolution of lithium polysulfides into the electrolyte from the sulfur cathode during cycling. It is noticeable that cells without additives showed a drastic increase in electrolyte resistance, whereas the cell with $Fe_{1-x}S$@NC exhibited a small increase in electrolyte resistance. This result suggests that a lower amount of lithium polysulfides are dissolved into the electrolyte in cells with $Fe_{1-x}S$@NC, because $Fe_{1-x}S$@NC particles can effectively trap lithium polysulfides within the sulfur cathode. The

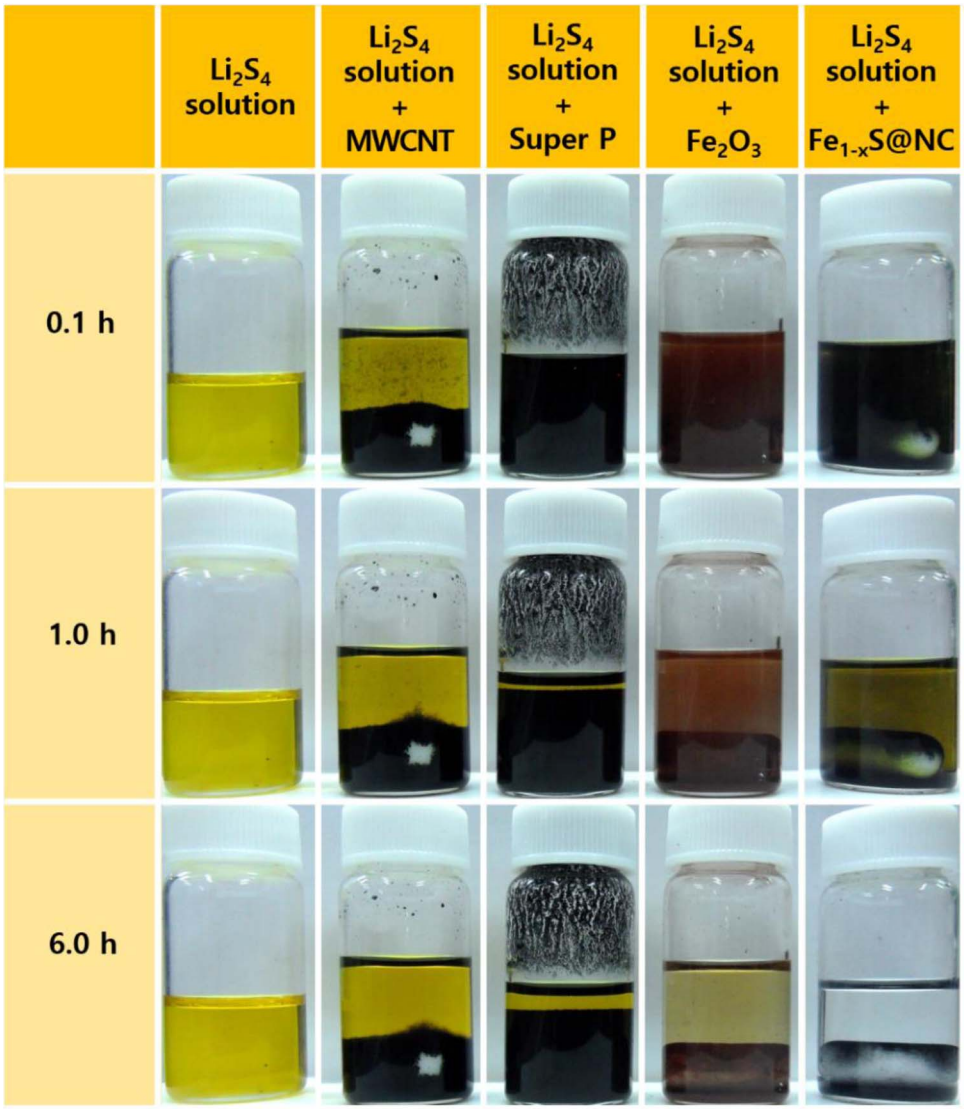

Figure 4. Photographs of Li_2S_4 solutions containing MWCNT, Super-P, Fe_2O_3 and $Fe_{1-x}S$@NC after stirring for 0.1, 1.0 and 6.0 h, respectively.

interfacial resistances in cell without additives were also significantly increased after 300 cycles. This is because the dissolution and migration of polysulfides to the anode side causes the degradation of interfacial contacts in the sulfur cathode and the retardation of the charge transfer reaction at the electrode-electrolyte interface. In addition, the migrated lithium polysulfides could be deposited on the surface of the lithium anode, resulting in an increase of surface film resistance. In contrast, the cell with $Fe_{1-x}S$@NC showed a relatively small increase in interfacial resistances after 300 cycles, resulting in the lowest cell resistance among the cells investigated. These results demonstrate that the addition of $Fe_{1-x}S$@NC with good adsorption ability for polysulfides and high electronic conductivity effectively traps and reutilizes lithium polysulfides within the cathode side, resulting in superior cycling performance as compared with the other two cells.

The rate capability of the Li-sulfur cell with different sulfur cathodes was evaluated at various C rates. In the rate capability test, the cells were charged and discharged at different current rates with increasing current rate from 0.1 to 5.0 C every five cycles. Figure 8a shows the charge and discharge curves of the Li-sulfur cell with $Fe_{1-x}S$@NC at different C rates, plotted for the first cycle at each C rate. With increasing current rate, the overpotential increased and the discharge capacity was decreased with shortening discharge plateaus. From the cycling of cells with different cathodes at various current rates, their rate performance is compared (Figure 8b). Clearly, the Li-sulfur cell with $Fe_{1-x}S$@NC delivered the highest discharge capacities at all C rates. The enhanced high-rate performance can be attributed to suppression of polysulfide dissolution due to effective trapping by $Fe_{1-x}S$@NC and enhanced electronic conductivity. Although Fe_2O_3 particles have a little ability to adsorb lithium polysulfides, as demonstrated in Figure 4, their insulating nature significantly reduce the discharge capacity during the lower discharge plateau at high current rates. As a result, the discharge capacity of the cell with Fe_2O_3 was dropped from 938.4 to 84.9 mAh g^{-1} when the current rate was increased from 0.1 to 5.0 C. The Li-sulfur cell with $Fe_{1-x}S$@NC recovered its discharge capacity when the C rate was decreased from 5.0 to 0.1C. These results suggest that the addition of $Fe_{1-x}S$@NC into the sulfur cathode not only increases cycling stability but also improves the rate capability of Li-sulfur cells.

Conclusions

$Fe_{1-x}S$ uniformly coated by N-doped carbon ($Fe_{1-x}S$@NC) was synthesized and used as an additive for chemical confinement of lithium polysulfides in Li-sulfur cells. The addition of $Fe_{1-x}S$@NC into the sulfur cathode not only suppressed the migration of lithium

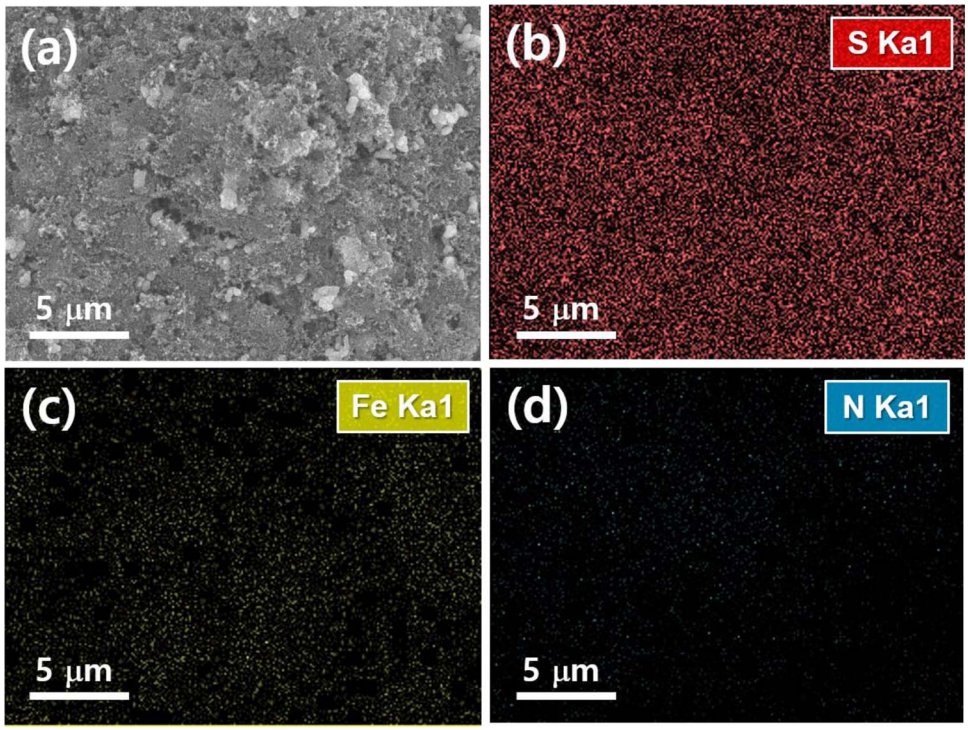

Figure 5. (a) SEM image of the sulfur electrode containing $Fe_{1-x}S$@NC particles and its EDS elemental mappings corresponding to (b) S, (c) Fe and (d) N.

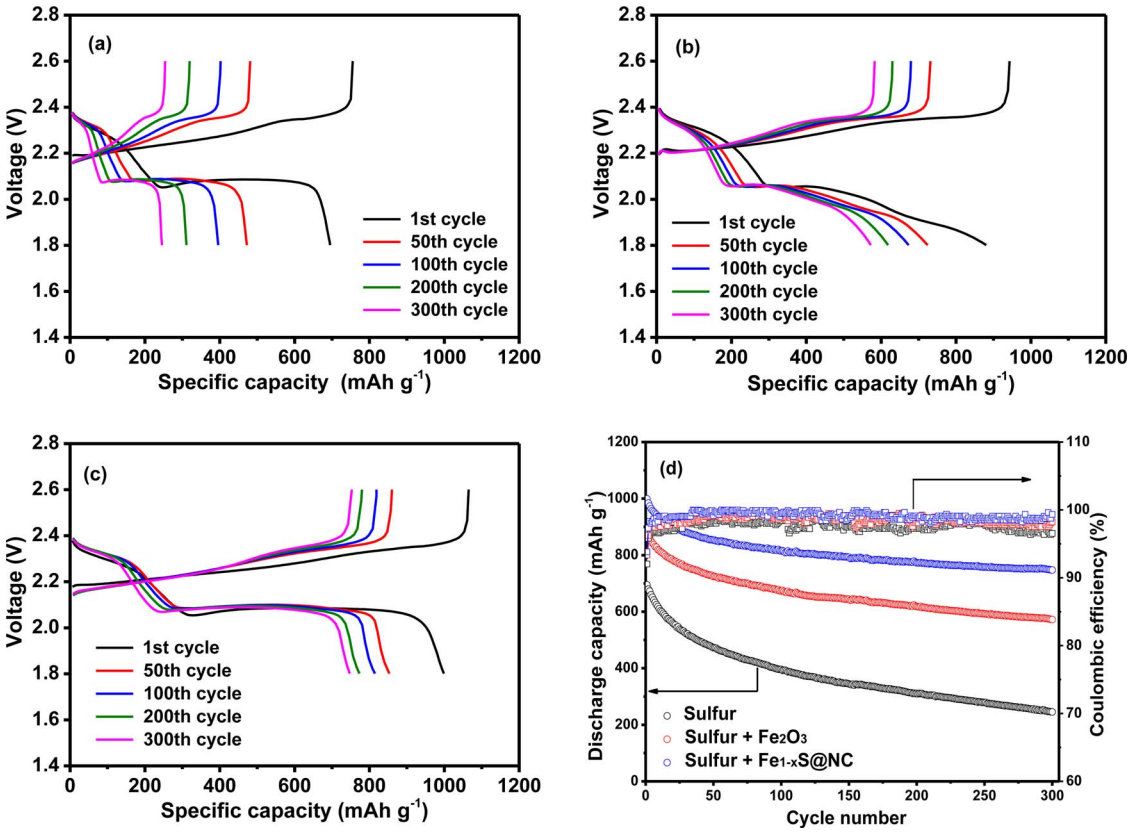

Figure 6. Charge and discharge voltage profiles of the Li-sulfur cells assembled with different sulfur cathodes at constant current rate of 0.2 C. (a) Sulfur without additives, (b) sulfur with Fe_2O_3 and (c) sulfur with $Fe_{1-x}S$@NC. (d) Discharge capacities and coulombic efficiencies of the Li-sulfur cells with different sulfur cathodes at 0.2 C rate as a function of cycle number.

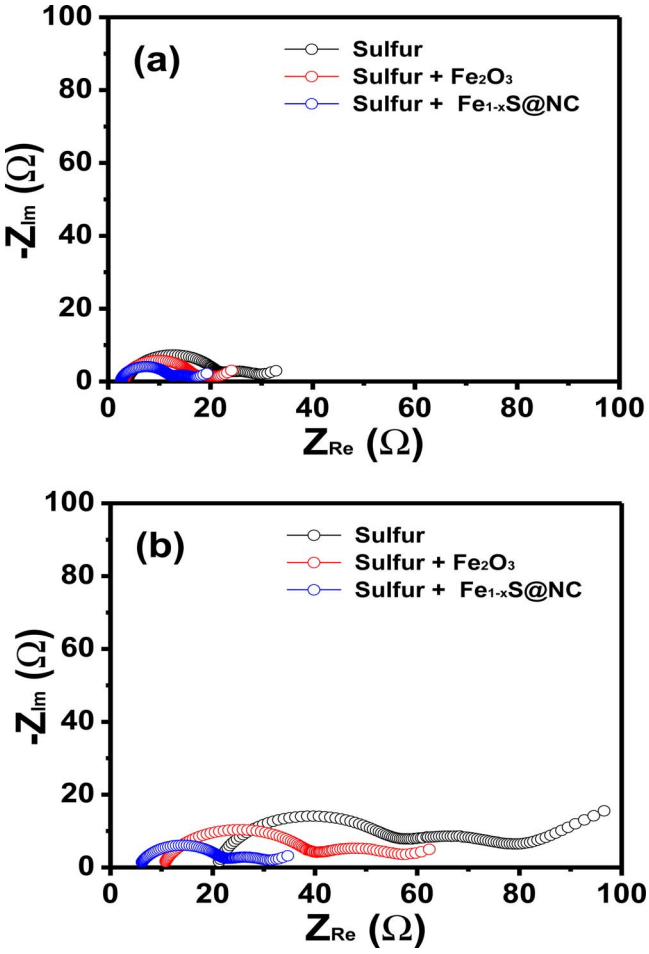

Figure 7. AC impedance spectra of the Li-sulfur cells with different sulfur cathodes after (a) the 1st and (b) 300th cycles.

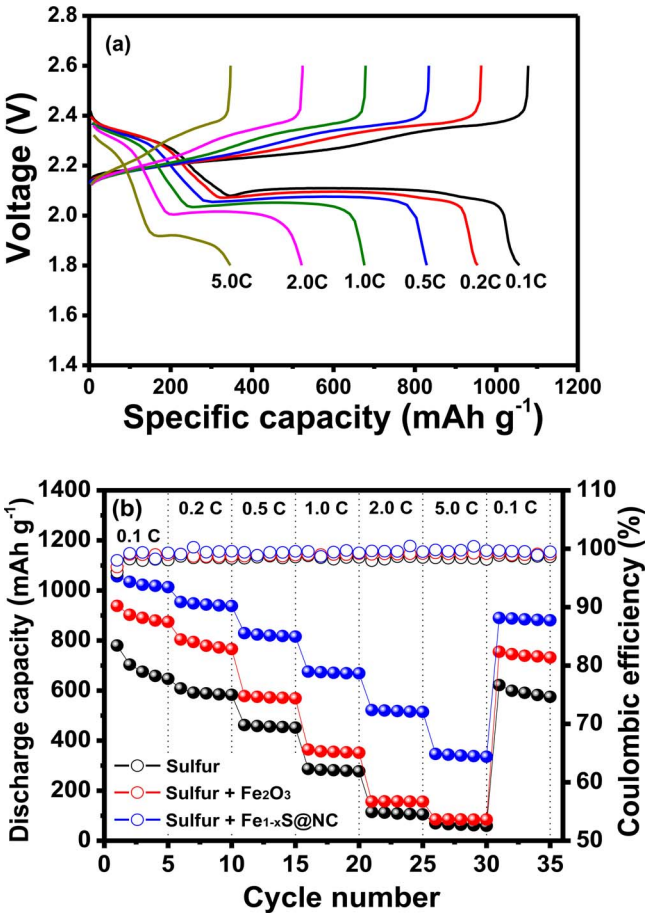

Figure 8. (a) Charge and discharge profiles of the Li-sulfur cell assembled with $Fe_{1-x}S$@NC at various C rates, and (b) discharge capacities and coulombic efficiencies of the Li-sulfur cells with the C rate increasing from 0.1 to 5.0 C every five cycles.

polysulfides toward lithium anode by effectively trapping polysulfides but also enhanced the electronic conductivity for reutilization of trapped lithium polysulfides within the sulfur cathode. As a result, the Li-sulfur cell with $Fe_{1-x}S$@NC delivered a high initial discharge capacity of 999.0 mAh g^{-1} with good capacity retention and exhibited an enhanced rate capability. Further tailoring the morphology of such additive materials would provide a more beneficial effect on the cycling performance of Li-sulfur cells.

Acknowledgments

This work was supported by the Basic Science Research Program of the National Research Foundation of Korea (NRF), funded by the Ministry of Science, ICT, and Future Planning (2017R1A2A2A05020947) and the Technology Innovation Program funded by the Ministry of Trade, Industry and Energy (MOTIE, Korea) (10069215).

ORCID

Dong-Won Kim https://orcid.org/0000-0002-1735-0272

References

1. M. Armand and J. M. Tarascon, *Nature*, **451**, 652 (2008).
2. P. G. Bruce, S. A. Freunberger, L. J. Hardwick, and J.-M. Tarascon, *Nat. Mater.*, **11**, 19 (2012).
3. D. Eroglu, K. R. Zavadil, and K. G. Gallagher, *J. Electrochem. Soc.*, **162**, A982 (2015).
4. X. Ji and L. F. Nazar, *J. Mater. Chem.*, **20**, 9821 (2010).
5. A. Manthiram, Y. Fu, S.-H. Chung, C. Zu, and Y.-S. Su, *Chem. Rev.*, **114**, 11751 (2014).
6. Y.-X. Yin, S. Xin, Y.-G. Guo, and L.-J. Wan, *Angew. Chem. Int. Edit.*, **52**, 13186 (2013).
7. S. S. Zhang, *J. Power Sources*, **231**, 153 (2013).
8. X. Ji, K. T. Lee, and L. F. Nazar, *Nat. Mater.*, **8**, 500 (2009).
9. G. Zheng, Y. Yang, J. J. Cha, S. S. Hong, and Y. Cui, *Nano Lett.*, **11**, 4462 (2011).
10. S. Lu, Y. Cheng, X. Wu, and J. Liu, *Nano Lett.*, **13**, 2485 (2013).
11. X. Liang, Z. Wen, Y. Liu, H. Zhang, L. Huang, and J. Jin, *J. Power Sources*, **196**, 3655 (2011).
12. N. Jayaprakash, J. Shen, S. S. Moganty, A. Corona, and L. A. Archer, *Angew. Chem. Int. Edit.*, **50**, 5904 (2011).
13. H. Chen, W. Dong, J. Ge, C. Wang, X. Wu, W. Lu, and L. Chen, *Sci. Rep.*, **3**, 1910 (2013).
14. J. Lee and W. Choi, *J. Electrochem. Soc.*, **162**, A935 (2015).
15. Y. Sun, G. Li, Y. Lai, D. Zeng, and H. Cheng, *Sci. Rep.*, **6**, 22048 (2016).
16. S. Moon, J.-K. Yoo, Y. H. Jung, J.-H. Kim, Y. S. Jung, and D. K. Kim, *J. Electrochem. Soc.*, **164**, A6417 (2017).
17. R. Ponraj, A. G. Kannan, J. H. Ahn, and D.-W. Kim, *ACS Appl. Mater. & Inter.*, **8**, 4000 (2016).
18. B. Campbell, J. Bell, H. Hosseini Bay, Z. Favors, R. Ionescu, C. S. Ozkan, and M. Ozkan, *Nanoscale*, **7**, 7051 (2015).
19. J. He, L. Luo, Y. Chen, and A. Manthiram, *Adv. Mater.*, **29**, 1702707 (2017).
20. X. Ji, S. Evers, R. Black, and L. F. Nazar, *Nat. Commun.*, **2**, 325 (2011).
21. Z. W. Seh, J. H. Yu, W. Li, P.-C. Hsu, H. Wang, Y. Sun, H. Yao, Q. Zhang, and Y. Cui, *Nat. Commun.*, **5**, 5017 (2014).
22. Y. Peng, Y. Zhang, J. Huang, Y. Wang, H. Li, B. J. Hwang, and J. Zhao, *Carbon*, **124**, 23 (2017).
23. X. Wu, L. Fan, M. Wang, J. Cheng, H. Wu, B. Guan, N. Zhang, and K. Sun, *ACS Appl. Mater. & Inter.*, **9**, 18889 (2017).
24. J. Zhang, Y. Shi, Y. Ding, L. Peng, W. Zhang, and G. Yu, *Adv. Energy Mater.*, **7**, 1602876 (2017).
25. W. Cai, J. Zhou, G. Li, K. Zhang, X. Liu, C. Wang, H. Zhou, Y. Zhu, and Y. Qian, *ACS Appl. Mater. & Inter.*, **8**, 27679 (2016).

26. R. Ponraj, A. G. Kannan, J. H. Ahn, J. H. Lee, J. Kang, B. Han, and D.-W. Kim, *ACS Appl. Mater. & Inter.*, **9**, 38445 (2017).
27. W. Qin, S. Lu, Z. Wang, and X. Wu, *J. Energy Chem.*, **26**, 448 (2017).
28. S. A. Ahad, P. R. Kumar, J.-H. Kim, D. J. Kim, P. Ragupathy, and D. K. Kim, *Electrochim. Acta*, **246**, 451 (2017).
29. Z. Meng, Y. Xie, T. Cai, Z. Sun, K. Jiang, and W.-Q. Han, *Electrochim. Acta*, **210**, 829 (2016).
30. X. Liang, C. Y. Kwok, F. Lodi-Marzano, Q. Pang, M. Cuisinier, H. Huang, C. J. Hart, D. Houtarde, K. Kaup, H. Sommer, T. Brezesinski, J. Janek, and L. F. Nazar, *Adv. Energy Mater.*, **6**, 1501636 (2016).
31. Q. Pang, D. Kundu, M. Cuisinier, and L. F. Nazar, *Nat. Commun.*, **5**, 4759 (2014).
32. H. Yao, G. Zheng, P.-C. Hsu, D. Kong, J. J. Cha, W. Li, Z. W. Seh, M. T. McDowell, K. Yan, Z. Liang, V. K. Narasimhan, and Y. Cui, *Nat. Commun.*, **5**, 3943 (2014).
33. X. Tao, J. Wang, C. Liu, H. Wang, H. Yao, G. Zheng, Z. W. Seh, Q. Cai, W. Li, G. Zhou, C. Zu, and Y. Cui, *Nat. Commun.*, **7**, 11203 (2016).
34. R. V. Bugga, S. C. Jones, J. Pasalic, C. S. Seu, J.-P. Jones, and L. Torres, *J. Electrochem. Soc.*, **164**, A265 (2017).
35. K. Sun, C. A. Cama, R. A. DeMayo, D. C. Bock, X. Tong, D. Su, A. C. Marschilok, K. J. Takeuchi, E. S. Takeuchi, and H. Gan, *J. Electrochem. Soc.*, **164**, A6039 (2017).
36. Q. Zhang, D. C. Bock, K. J. Takeuchi, A. C. Marschilok, and E. S. Takeuchi, *J. Electrochem. Soc.*, **164**, A897 (2017).
37. U. Ulissi, S. Ito, S. M. Hosseini, A. Varzi, Y. Aihara, and S. Passerini, *Adv. Energy. Mater.* **8**, 1801462 (2018).
38. J. Barker and E. Kendrick, *J. Power Sources*, **196**, 6960 (2011).
39. R. Fong and J. R. Dahn, *J. Electrochem. Soc.*, **136**, 3206 (1989).
40. L. Li, S. Peng, N. Bucher, H. Y. Chen, N. Shen, A. Nagasubramanian, E. Eldho, S. Hartung, S. Ramakrishna, and M. Srinivasan, *Nano Energy*, **37**, 81 (2017).
41. C. Xu, Y. Zeng, X. Rui, N. Xiao, J. Zhu, W. Zhang, J. Chen, W. Liu, H. Tan, H. H. Hng, and Q. Yan, *ACS Nano*, **6**, 4713 (2012).
42. B. Wu, H. Song, J. Zhou, and X. Chen, *Chem. Commun.*, **47**, 8653 (2011).
43. A. Naitabdi, L. K. Ono, F. Behafarid, and B. R. Cuenya, *J. Phys. Chem. C*, **113**, 1433 (2009).
44. Y. He, P. Xu, B. Zhang, Y. Du, B. Song, X. Han, and H. Peng, *ACS Appl. Mater. Interfaces*, **9**, 38401 (2017).
45. G. K. Veerasubramani, Y. Subramaniam, M.-S. Park, G. Nagaraju, B. Senthilumar, Y. S. Lee, and D.-W. Kim, *J. Mater. Chem. A*, **6**, 20056 (2018).
46. Y. Tan, K.-W. Wong, Z. Zhang, and K. M. Ng, *Nanoscal*e, **9**, 19408 (2017).
47. C. I. Pearce, R. A. D. Pattrick, and D. J. Vaughan, *Rev Mineral Geochem*, **61**, 127 (2006).
48. J. Moskon, R. Dominko, R. Cerc-Korosec, M. Gaberscek, and J. Jamnik, *J. Power Sources*, **174**, 683 (2007).